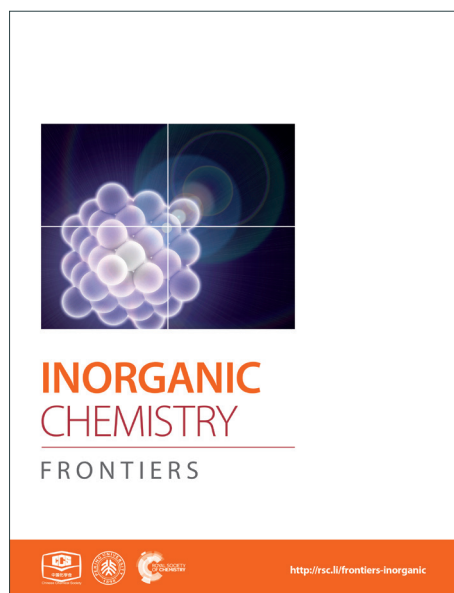
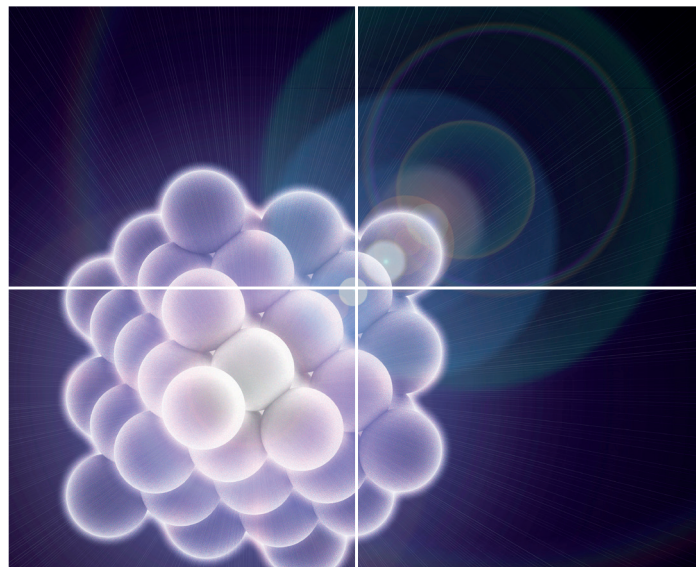


INORGANIC CHEMISTRY

FRONTIERS

Accepted Manuscript



This is an *Accepted Manuscript*, which has been through the Royal Society of Chemistry peer review process and has been accepted for publication.

Accepted Manuscripts are published online shortly after acceptance, before technical editing, formatting and proof reading. Using this free service, authors can make their results available to the community, in citable form, before we publish the edited article. We will replace this *Accepted Manuscript* with the edited and formatted *Advance Article* as soon as it is available.

You can find more information about *Accepted Manuscripts* in the [Information for Authors](#).

Please note that technical editing may introduce minor changes to the text and/or graphics, which may alter content. The journal's standard [Terms & Conditions](#) and the [Ethical guidelines](#) still apply. In no event shall the Royal Society of Chemistry be held responsible for any errors or omissions in this *Accepted Manuscript* or any consequences arising from the use of any information it contains.

Synthesis, Polymorphism, and Electronic Structures of $\text{Sr}_3\text{Sn}_2\text{As}_4$

Cite this: DOI: 10.1039/x0xx00000x

Xiao-Cun Liu,^a Ming-Yan Pan,^a Xin Li,^a Sheng-Qing Xia,^{*a} and Xu-Tang Tao^a

Received,
Accepted

DOI: 10.1039/x0xx00000x

rsc.li/frontiers-inorganic

Two polymorphs of $\text{Sr}_3\text{Sn}_2\text{As}_4$ have been synthesized from the Sn-flux reactions, and their structures were determined by single-crystal X-ray diffraction technique. α - $\text{Sr}_3\text{Sn}_2\text{As}_4$ adopts the $\text{Sr}_3\text{Sn}_2\text{P}_4$ structure type with the orthorhombic space group $Cmca$ ($a = 25.798(2)$ Å, $b = 12.8883(11)$ Å, $c = 19.1244(16)$ Å, $V = 6358.8(9)$ Å³, $Z = 24$), whereas β - $\text{Sr}_3\text{Sn}_2\text{As}_4$ belongs to $\text{Ca}_3\text{Si}_2\text{As}_4$ structure type and crystallizes in the monoclinic crystal system $P2_1/c$ ($a = 7.7049(13)$, $b = 19.118(3)$, $c = 7.6877(13)$, $\beta = 112.003(2)^\circ$, $V = 1049.9(3)$, $Z = 4$). Despite the obvious structures differences, the polyanion units of both compounds feature similar $[\text{Sn}_2\text{As}_6]$ octahedron. Differential thermal analysis and thermogravimetry measurements indicate that α - $\text{Sr}_3\text{Sn}_2\text{As}_4$ has good thermal stability and melt at 1185K, while β - $\text{Sr}_3\text{Sn}_2\text{As}_4$ starts to decompose above 800 K. Diffuse reflectance spectrum measurements proved both compounds had a band gap of about 0.9 eV, supported by the density functional calculations.

Introduction

Zintl phases are valence precise compounds formed among metals with very different electronegativities, such as alkali metals, alkali earth metals, and group 13-15 elements^{1,2}. Recently, Zintl phases are appealing to more and more scientists due to their diverse structures and rich physical properties, including superconductivity³⁻⁵, magnetoresistance⁶⁻⁸, mixed-valence^{9,10}, thermoelectricity¹¹⁻¹³ and so on. Numerous studies on the crystal and electronic structures, as well as related properties have been reported in the past decade¹⁴. Surprisingly, although so many compounds have been synthesized, the variety of such phases seems far from being exhausted.

For Zintl compounds with the general formula $A_3M_2Pn_4$ (A = alkaline-earth metals, Yb or Eu; M = group 12, 13 or 14 metals; Pn = pnictogen elements), various polyanion structures have been discovered, i.e., two-dimensional $[\text{Cd}_2\text{Sb}_4]^{6-}$ layers in $\text{Ba}_3\text{Cd}_2\text{Sb}_4$ ¹⁵, one-dimensional $[\text{In}_2\text{P}_4]^{6-}$ chains in $\text{Eu}_3\text{In}_2\text{P}_4$ ¹⁶ and zero-dimensional $[\text{Sn}_{12}\text{P}_{24}]^{36-}$ clusters in $\text{Sr}_3\text{Sn}_2\text{P}_4$ ¹⁷, which can all be rationalized using the Zintl-Klemm concept. The variety of the 3-2-4 family has aroused many studies involving the correlation between structures and properties. As part of such investigations, the $A_3Tt_2Pn_4$ ($Tt = \text{Si, Ge or Sn}$) system is of special interest due to its structural diversity. The structures of $A_3Tt_2Pn_4$ generally feature polyanionic rings, such as four-membered rings in $\text{Sr}_3\text{Si}_2\text{As}_4$ ¹⁸, five-membered rings in $\text{Ca}_3\text{Si}_2\text{As}_4$ ¹⁹ and six-membered rings in $\text{Sr}_3\text{Sn}_2\text{P}_4$ ¹⁷. More interestingly, all these different rings are composed of the same Tt_2Pn_6 octahedral units.

Herein, we presented the flux synthesis of two new ternary Zintl polymorphs, α - $\text{Sr}_3\text{Sn}_2\text{As}_4$ and β - $\text{Sr}_3\text{Sn}_2\text{As}_4$, which belong to the $\text{Sr}_3\text{Sn}_2\text{P}_4$ ¹⁷ and $\text{Ca}_3\text{Si}_2\text{As}_4$ ¹⁹ structure types, respectively. Compounds with the $\text{Ca}_3\text{Si}_2\text{As}_4$ structure type are very common and more than half of the $A_3Tt_2Pn_4$ series adopt this structure. However, for the $\text{Sr}_3\text{Sn}_2\text{P}_4$ structure type, only one phosphide, $\text{Sr}_3\text{Sn}_2\text{P}_4$, was reported so far. By using single-crystal X-ray diffraction methods, the crystal structures of α - $\text{Sr}_3\text{Sn}_2\text{As}_4$ and β - $\text{Sr}_3\text{Sn}_2\text{As}_4$ were determined accurately, and in corporation with the density functional theoretical calculations their electronic structures were studied as well. The theoretical results indicated the semiconducting properties of both compounds, which were consistent with the measured optical diffuse reflectance spectrum data. Thermal stability studies were provided with the aid of differential thermal analysis and thermogravimetry measurements.

Results and Discussion

Structure Description

Compound α - $\text{Sr}_3\text{Sn}_2\text{As}_4$ crystallizes in the orthorhombic $\text{Sr}_3\text{Sn}_2\text{P}_4$ structure type ($Cmca$), whereas the β - $\text{Sr}_3\text{Sn}_2\text{As}_4$ crystallizes in the monoclinic $\text{Ca}_3\text{Si}_2\text{As}_4$ structure type ($P2_1/c$). Since the structures of both compounds have been well discussed in previous references, only some important structural features will be discussed here. Information on data collection, structure solution and refinement are summarized in Table 1. Positional and equivalent isotropic displacement parameters, selected bond distances are all listed in Table S1 and Table S2 (Supporting Information).

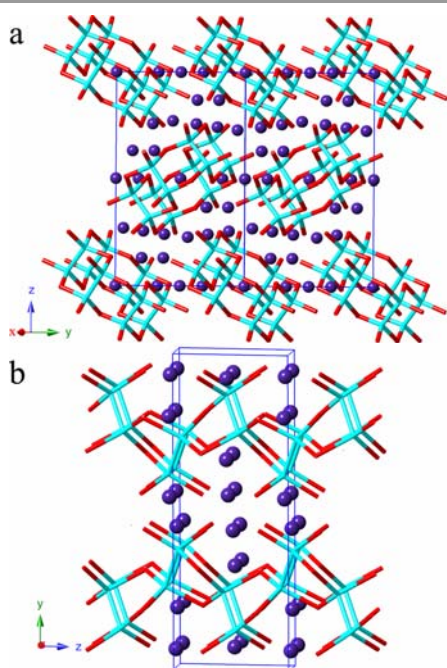


Figure 1. (a) Polyhedral and ball-and-stick representation of the crystal structure for α - $\text{Sr}_3\text{Sn}_2\text{As}_4$ viewed down the b -axis, $[\text{Sn}_{12}\text{As}_{24}]^{36-}$ clusters was emphasized in a polyhedral view. All unique atoms are indicated in graph and Sr, Sn and As atoms are plotted as purple, light blue and red spheres, respectively. (b) Ball-and-stick representation of the crystal structure of β - $\text{Sr}_3\text{Sn}_2\text{As}_4$, viewed down the a -axis, and the unit cell is outlined.

A structure comparison between α - $\text{Sr}_3\text{Sn}_2\text{As}_4$ and β - $\text{Sr}_3\text{Sn}_2\text{As}_4$ is provided in Figure 1. As shown in the picture, the anion structure of α - $\text{Sr}_3\text{Sn}_2\text{As}_4$ features an interesting $[\text{Sn}_{12}\text{As}_{24}]^{36-}$ cluster, which encapsulates a Sr^{2+} cation in the center. Each $[\text{Sn}_{12}\text{As}_{24}]^{36-}$ cluster can be viewed as composed of six $[\text{Sn}_2\text{As}_6]$ octahedra, connected in the edge-sharing manner. Such an ethane-like $[\text{Sn}_2\text{As}_6]$ fragment is very common in pnictide Zintl phases and similar examples have been frequently reported as in $\text{Sr}_3\text{Si}_2\text{As}_4$ ¹⁸, $\text{Ca}_3\text{Si}_2\text{As}_4$ ¹⁹ and ACdGeAs_2 ($A = \text{K}, \text{Rb}$)²⁰. However, it is really interesting if this structure is compared with its polymorph β - $\text{Sr}_3\text{Sn}_2\text{As}_4$, in which the polyanion structure turns out to be a completely different infinite chain. In addition, such one-dimension chains are also built of the same $[\text{Sn}_2\text{As}_6]$ octahedra as in α - $\text{Sr}_3\text{Sn}_2\text{As}_4$ and the connection of these $[\text{Sn}_2\text{As}_6]$ octahedral units still embodies the edge-sharing fashion. A better illustration on the difference in the anion structures of these two polymorphs is presented in Figure 2, shown by both polyhedral and ball-and-stick fashions. In α - $\text{Sr}_3\text{Sn}_2\text{As}_4$, the edge-sharing connection between two neighbouring $[\text{Sn}_2\text{As}_6]$ octahedra takes place *via* two As atoms shared by four different $[\text{SnAs}_3]$ triangular pyramids. This connection manner results in a unique $[\text{Sn}_4\text{As}_2]$ six-membered ring, which helps build the “circle-like” anion clusters in α - $\text{Sr}_3\text{Sn}_2\text{As}_4$. While for β - $\text{Sr}_3\text{Sn}_2\text{As}_4$ the situation is a little different: these two As atoms are shared by three $[\text{SnAs}_3]$ triangular pyramids, which are still from two different $[\text{Sn}_2\text{As}_6]$ octahedral and in this way, polyanion chains are formed featuring new $[\text{Sn}_3\text{As}_2]$ five-membered rings.

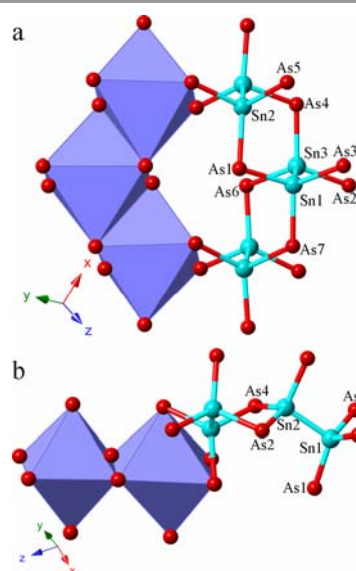


Figure 2. Polyhedral and ball-and-stick view of the structure of polyanion units of (a) α - $\text{Sr}_3\text{Sn}_2\text{As}_4$ and (b) β - $\text{Sr}_3\text{Sn}_2\text{As}_4$. Sr, Sn and As atoms are plotted as purple, light blue and red spheres, respectively. $[\text{Sn}_2\text{As}_6]$ octahedra are emphasized in polyhedral view.

Table 1. Selected crystal data and structure refinement parameters for two polymorphs of $\text{Sr}_3\text{Sn}_2\text{As}_4$

Formula	α - $\text{Sr}_3\text{Sn}_2\text{As}_4$	β - $\text{Sr}_3\text{Sn}_2\text{As}_4$
Fw / $\text{g}\cdot\text{mol}^{-1}$	799.92	799.92
T / K	296(2)	296(2)
Radiation, wavelength	Mo-K α , 0.71073 Å	
Crystal system	Orthorhombic	Monoclinic
Space group, Z	$Cmca$, 24	$P2_1/c$, 4
Unit cell dimensions		
a / Å	25.798(2)	7.7049(13)
b / Å	12.8883(11)	19.118(3)
c / Å	19.1244(16)	7.6877(13)
β / °	-	112.003(2)
V / Å ³	6358.8(9)	1049.9(3)
ρ_{calc} / $\text{g}\cdot\text{cm}^{-3}$	5.013	5.060
$\mu_{\text{Mo K}\alpha}$ / mm^{-1}	31.968	32.268
Extinction coefficient	0.000069(2)	-
GOF	1.019	1.050
Final R indices	$R_1 = 0.0329$	$R_1 = 0.0324$
^a [$>2\sigma(I)$]	$wR_2 = 0.0513$	$wR_2 = 0.0795$
Final R indices	$R_1 = 0.0610$	$R_1 = 0.0408$
^a [all data]	$wR_2 = 0.0667$	$wR_2 = 0.0831$

^a $R_1 = \sum||F_o| - |F_c|| / \sum|F_o|$; $wR_2 = [\sum[w(F_o^2 - F_c^2)^2] / \sum[w(F_o^2)^2]]^{1/2}$, and $w = 1 / [\sigma^2 F_o^2 + (A \cdot P)^2 + B \cdot P]$, $P = (F_o^2 + 2F_c^2) / 3$; A and B are weight coefficients.

The Sr cations are six-coordinated in both compounds, which all reside in the centers of the distorted As_6 octahedra. The Sn-Sn and Sn-As bonding distances are very similar as well in these two polymorphs. The corresponding Sn-Sn contacts are 2.7659(9) to 2.7955(12) Å in α - $Sr_3Sn_2As_4$, and 2.7173(9) Å in β - $Sr_3Sn_2As_4$. The Sn-As interatomic distances are in the ranges of 2.5523(10) to 2.6563(9) Å in α - $Sr_3Sn_2As_4$, and 2.5327(11) to 2.6362(10) Å in β - $Sr_3Sn_2As_4$. These results are comparable to those Zintl compounds with similar bonding patterns²¹⁻²³, yet much shorter than the typical multicenter bonding distances^{24, 25}. This is consistent with the Zintl concept that the interactions of anionic structures should be localized two-center two-electron (2c-2e) bonding. The As-Sn-Sn bonding angles are in the range of 103.59(4)° to 111.73(3)° in α - $Sr_3Sn_2As_4$ and 97.24(3)° to 117.87(3)° in β - $Sr_3Sn_2As_4$, which suggests an obviously more distorted tetrahedral coordination geometry for the Sn atoms in β - $Sr_3Sn_2As_4$ due to the formation of the five-membered rings.

Thermal stability

TG-DSC measurements were performed in order to evaluate the thermal stability of both compounds, and the results are shown in Figure S1 (Supporting Information). There is no obvious phase transition behavior observed between these two phases. For α - $Sr_3Sn_2As_4$, two sequential cycles were performed to ensure its thermal behavior and the results of the 2nd cycle were shown in Figure S2. There is no significant mass loss observed in the whole measured process. Both two DSC curves exhibit similarly sharp endothermic peaks and exothermic peaks at 1185 K and 1160 K, respectively. Due to the good reproducibility, these two peaks should be attributed to melting and crystallization processes of this compound. Although based on the powder diffraction patterns (Figure S3) there are no significant impurities identified, the slight fluctuations of the curves suggest the possible existence of some uncertain amorphous impurities. Similar situation exists for β - $Sr_3Sn_2As_4$, however, a significant mass loss is observed at above 800 K, which evidently indicates the decomposition process of β - $Sr_3Sn_2As_4$. It is not surprising that both compounds have shown distinct thermal behavior due to their different structures. The thermal behavior of β -phase is very similar to its isostructural analogue $Eu_3Ge_2As_4$ ²⁶, which also has a mass loss of about 7% in the range from 830K to 1170K.

Optical Absorption Spectrum

UV-vis/near-IR diffuse reflectance spectra were recorded at room temperature for both α - $Sr_3Sn_2As_4$ and β - $Sr_3Sn_2As_4$ and the calculated optical absorption spectra are presented in Figure S4. The optical absorption spectra of compounds are very similar and both suggest semiconducting character. The room temperature band gaps evaluated for α - $Sr_3Sn_2As_4$ and β - $Sr_3Sn_2As_4$ are 0.86(2) and 0.87(3) eV, respectively, which are consistent with their black colour. However, as mentioned above, the existence of some uncertain amorphous impurities may also affect the absorption behavior, which exhibit a small peak around 0.9 eV as well as the fluctuant baseline. Tauc plots

were also tried to evaluate the band gaps (Figure S5) and the results are consistent with the previous findings.

Electronic Band Structure

To better understand their optical properties, electronic band structure calculations based on the density functional method were carried out for both compounds and the results are shown in Figure 3. As seen from the picture, both structures clearly indicate the existence of a small band gap, 0.82 and 0.83 eV for α - $Sr_3Sn_2As_4$ and β - $Sr_3Sn_2As_4$, respectively, which suggest semiconducting character as confirmed by the optical absorption spectra above. In addition, the valence band maximum (VBM) and the conduction band minimum (CBM) of the compounds are both located at the same k -vector, a clue that these compounds should be direct band gap semiconductors. Despite the similarities, the band structures of α - $Sr_3Sn_2As_4$ and

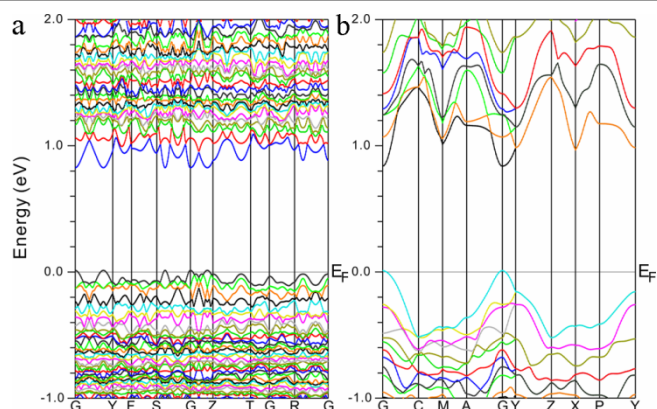


Figure 3. Calculated electronic band structures for (a) α - $Sr_3Sn_2As_4$ and (b) β - $Sr_3Sn_2As_4$, respectively. The Fermi level is chosen as the energy reference at 0 eV.

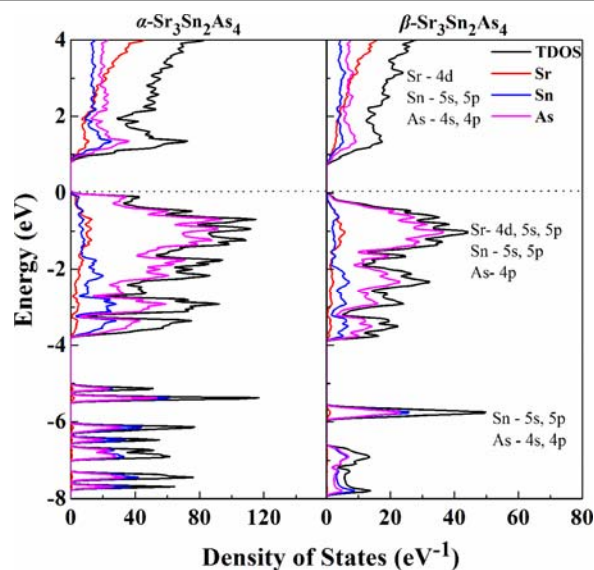


Figure 4. Calculated total DOS and projected DOS are plotted on the same energy scale for α - $Sr_3Sn_2As_4$ and β - $Sr_3Sn_2As_4$. The Fermi level is selected as the energy reference.

β - $\text{Sr}_3\text{Sn}_2\text{As}_4$ are significantly different in the band width. The bands in α - $\text{Sr}_3\text{Sn}_2\text{As}_4$ are obviously much narrower than those of β - $\text{Sr}_3\text{Sn}_2\text{As}_4$, which means the electrons are more localized in α - $\text{Sr}_3\text{Sn}_2\text{As}_4$ than in β - $\text{Sr}_3\text{Sn}_2\text{As}_4$. By taking their crystal structures into account, such discrepancies are reasonable since in α - $\text{Sr}_3\text{Sn}_2\text{As}_4$, the polyanion structure is basically composed of the isolated $[\text{Sn}_{12}\text{As}_{24}]^{36-}$ clusters, whereas for β - $\text{Sr}_3\text{Sn}_2\text{As}_4$ the Sn and As atoms form infinite chains in favor of electron transport.

Projections of the corresponding total and partial density of states (DOS) for both α - $\text{Sr}_3\text{Sn}_2\text{As}_4$ and β - $\text{Sr}_3\text{Sn}_2\text{As}_4$ are presented in Figure 4. A qualitative comparison of the DOS between these two polymorphs reveals high similarity in the DOS curves: the conduction bands are generally composed of 4d orbits of Sr and the antibonding states originated from the Sn-As interactions; the valence bands can be divided into two different regions—the lower region ranging from -8 to -4 eV are primarily contributed by the localized s states from As atoms and another region, which has relatively higher energy below the Fermi level, is composed mainly of Sr-4d, Sn-5s and 5p, and As-4p orbitals. The highly hybridization between Sn and As orbitals in valence band suggests strong covalent interactions within the anionic framework and the significant p-d mixing of Sr and As indicates non-negligible covalent bonding interactions between cations and anions. Although cations in Zintl phases are usually considered merely as charge suppliers and space fillers, many recent researches²⁷⁻²⁹ indicate that they can play more important roles, such as stabilizing the structure or affecting the transport properties. Despite the similarities above, there exist a sharp shoulder peak right below the Fermi level for α - $\text{Sr}_3\text{Sn}_2\text{As}_4$, which predominantly consists of the 4p orbitals of As atoms and is not observed in β - $\text{Sr}_3\text{Sn}_2\text{As}_4$. This peak should be designated as the non-bonding electrons or lone pair on As atoms of α - $\text{Sr}_3\text{Sn}_2\text{As}_4$ with the knowledge that the polyanion structure of α - $\text{Sr}_3\text{Sn}_2\text{As}_4$ consist of the isolated $[\text{Sn}_{12}\text{As}_{24}]^{36-}$ clusters, which should more favor the electron localization than the chain structure of β - $\text{Sr}_3\text{Sn}_2\text{As}_4$. These results are in accord with the electronic band structure calculations presented above and as well are similar to our recent report on arsenide Zintl analogues.^{30,31}

Conclusions

In conclusion, two polymorphs of $\text{Sr}_3\text{Sn}_2\text{As}_4$ have been synthesized and structurally characterized. Although they feature identical $[\text{Sn}_2\text{As}_6]$ octahedral building units, the different connection manners lead to the significant different polyanionic structures. For α - $\text{Sr}_3\text{Sn}_2\text{As}_4$, the structure can be described as made up of zero-dimensional $[\text{Sn}_{12}\text{As}_{24}]^{36-}$ clusters that are separated by the Sr cations and in β -phase there exist one dimensional infinite chains consisting of edge-sharing $[\text{Sn}_2\text{As}_6]$ octahedra. The measured optical absorption spectra for both compounds suggest semiconducting character with band gaps of 0.86 and 0.87 eV for α - $\text{Sr}_3\text{Sn}_2\text{As}_4$ and β - $\text{Sr}_3\text{Sn}_2\text{As}_4$, respectively. These results are in good agreement with the theoretical calculations.

Experimental Section

Synthesis

All syntheses were performed in an argon-filled glovebox with the oxygen level below 0.1 ppm or under vacuum. The elements were commercially purchased and used as received: Sr (Afla, granules, 99%), Sn (Alfa, shot, 99.9%), As (Alfa, lump, 99.999%).

α - $\text{Sr}_3\text{Sn}_2\text{As}_4$. Single crystals of α - $\text{Sr}_3\text{Sn}_2\text{As}_4$ were initially prepared by using the Sn as self-flux and big single crystal of α - $\text{Sr}_3\text{Sn}_2\text{As}_4$ were obtained by utilizing the following procedure: Sr:Sn:As = 3:10:4 were loaded into an alumina crucible and the reaction mixture was first heated to 1000 °C at a rate of 200 °C/h, then homogenized at this temperature for 20 h, and slowly cooled down to 600 °C at a rate of 3 °C/h. At this temperature, the ampule was quickly taken out of the furnace and the excess of Sn was removed by centrifuge. The utilization of low-fold metal flux (5-fold excess of Sn) is necessary in order to synthesize the α - $\text{Sr}_3\text{Sn}_2\text{As}_4$ and a high-fold metal flux, such as 20-fold excess or higher, will lead to another product $\text{Sr}_5\text{Sn}_2\text{As}_6$ ²¹. Stoichiometric reactions were also tried, but the main products of such reactions were mixtures of small irregular blocks of α - $\text{Sr}_3\text{Sn}_2\text{As}_4$ as well as some uncertain amorphous phases.

β - $\text{Sr}_3\text{Sn}_2\text{As}_4$. β - $\text{Sr}_3\text{Sn}_2\text{As}_4$ was accidentally identified from the Sn-flux reaction aiming at synthesizing a hypothetical compound “ SrSnAs_2 ” by using a loading ratio of Sr:Sn:As = 1:7:2. The synthesis process is similar to that of α - $\text{Sr}_3\text{Sn}_2\text{As}_4$ but a higher homogenization temperature (1050 °C) and lower flux separation temperature (500 °C) were applied. The products of this reaction consist of block-shaped α - $\text{Sr}_3\text{Sn}_2\text{As}_4$ and some plate-shaped crystals of β - $\text{Sr}_3\text{Sn}_2\text{As}_4$. After the crystal structure of β - $\text{Sr}_3\text{Sn}_2\text{As}_4$ was identified, several stoichiometric reactions attempting to synthesize β - $\text{Sr}_3\text{Sn}_2\text{As}_4$ were tried but the results were negative.

Single crystal structure determination

In order to avoid possible decomposition of the title compounds during the data collection, all crystals were picked in an argon-filled glovebox and cut in Paratone N oil to the desired dimensions. The X-ray diffraction data was collected on a Bruker CCD-based diffractometer at 296 K utilizing a Mo K α radiation (0.71703 Å). Data reduction and integration, together with global unit cell refinements were done by the INTEGRATE program incorporated in APEX2 software³². Semiempirical absorption corrections were applied using the SCALE program for area detector³². The structures were solved by direct methods and refined by full matrix least-squares methods on F² using SHELX³³. In the last refinement cycles, the atomic positions for the two compounds were standardized using the program Structure TIDY^{34,35}. All structures were refined to convergence with anisotropic displacement parameters. Crystallographic data and structural refinements are summarized in Table 1. Atomic positions and anisotropic displacement parameters and selected bond lengths

are given in Table 2 and Table 3, respectively. Further information in the form of CIF has been deposited with Fachinformationszentrum Karlsruhe, 76344 Eggenstein-Leopoldshafen, Germany, (fax: (49) 7247-808-666; e-mail: crysdata@fiz-karlsruhe.de) – depository CSD-428135 and 428136 for α -Sr₃Sn₂As₄ and β -Sr₃Sn₂As₄, respectively.

Powder X-ray diffraction

For phase identification, powder X-ray diffraction (PXRD) patterns were taken at room temperature by a Bruker AXS X-ray powder diffractometer using Cu-K α radiation. The data were recorded in a 2θ mode with a step size of 0.02° and a counting time of 10 s. In Figure S3 (in supporting information), the comparison between experimental and simulated data confirms the purity of the samples.

Differential Thermal Analysis and Thermogravimetry Measurements (DTA/TG)

The thermal stability of α -Sr₃Sn₂As₄ and β -Sr₃Sn₂As₄ were tested using a Mettler-Toledo TGA/DSC/1600HT instrument. Thermogravimetric Analysis (TGA) and Differential Scanning Calorimetry (DSC) experiments were performed on polycrystalline material samples for two phases under the protection of high-purity argon gas with a heating rate of 10 K/min. In order to verify the thermal behavior of the α -phase, the TG-DSC measured twice.

UV–Vis–NIR Diffuse Reflectance Spectrum

The optical diffuse reflectance spectrum for two polymorphs of Sr₃Sn₂As₄ were measured on polycrystalline samples at room temperature using a Shimadzu UV-3101 PC spectrometer equipped with an integrating sphere attachment and BaSO₄ as a reference. The absorption spectrum was calculated from the reflection spectrum via the Kubelka-Munk function: $\alpha/S = (1-R)^2/2R$, in which α was the absorption coefficient, S was the scattering coefficient, and R was the reflectance.

Computational details

The electronic band structure calculations of Sr₃Sn₂As₄ were performed with the full potential linearized augmented plane wave method (FP-LAPW)^{36,37} as implemented in the Wien2k code³⁸. In this method, the unit cell is divided into non-overlapping muffin-tin (MT) spheres and an interstitial region. The wavefunctions in the interstitial regions are expanded in plane waves up to $R_{MT} \times K_{max} = 7$, where R_{MT} is the smallest radius of all MT spheres and K_{max} the plane wave cut-off. The valence wavefunctions inside the MT spheres are expanded up to $l_{max}=10$ while the charge density was Fourier expanded up to $G_{max} = 12 \text{ au}^{-1}$. The MT radii were chosen to be 2.4 Bohr for Sr and Sn atoms and 2.3 Bohr for As atoms. Calculations were performed using 1000 k-points and the exchange correlation potential was calculated using the Perdew-Burke-Ernzerhof generalized gradient approximation (PBE-GGA)³⁹. The Brillouin Zone (BZ) integration was performed using the tetrahedron method and the self-consistent calculations were considered to have converged if the total energy and the charge

of the system are stable within 10⁻⁴ Ryd and 10⁻⁴ e⁻, respectively.

Acknowledgements

The authors acknowledge the financial support from the National Natural Science Foundation of China (Grant Nos. 51271098, 51021062, 51272129), the Independent Innovation Foundation of Shandong University (IIFSDU), the Program of Introducing Talents of Disciplines to Universities in China (111 program no. b06017).

Notes and references

^aState Key Laboratory of Crystal Materials, Institute of Crystal Materials, Shandong University, Jinan, Shandong 250100, People's Republic of China.

Email: shqxia@sdu.edu.cn

[†]Electronic Supplementary Information (ESI) available: The X-ray crystallographic file in CIF format of the title compounds; positional and equivalent isotropic displacement parameters and selected bond distances of two compounds; TG-DSC measurements on both compounds; the TG-DSC curves of 2nd cycle for α -Sr₃Sn₂As₄; powder X-ray diffraction patterns of the polycrystalline samples of two polymorphs of Sr₃Sn₂As₄; the optical absorption spectrum measured on polycrystalline samples. See DOI: 10.1039/b000000x/

- 1 E. Zintl, *Angew. Chem.*, 1939, **52**, 1–6.
- 2 S. M. Kauzlarich, *Chemistry, Structure and Bonding of Zintl Phases and Ions*, VCH Publishers, New York, 1996.
- 3 M. Rotter, M. Tegel and D. Johrendt, *Phys. Rev. Lett.*, 2008, **101**, 107006.
- 4 X. C. Wang, Q. Q. Liu, Y. X. Lv, W. B. Gao, L. X. Yang, R. C. Yu, F. Y. Li and C. Q. Jin, *Solid State Commun.*, 2008, **148**, 538–540.
- 5 T. Nomura, S. W. Kim, Y. Kamihara, M. Hirano, P. V. Sushko, K. Kato, M. Takata, A. L. Shluger and H. Hosono, *Supercond. Sci. Technol.*, 2008, **21**, 125028.
- 6 A. M. Goforth, H. Hope, C. L. Condon, S. M. Kauzlarich, N. Jensen, P. Klavins, S. MaQuilon and Z. Fisk, *Chem. Mater.*, 2009, **21**, 4480–4489.
- 7 D. J. Webb, R. Cohen, P. Klavins, R. N. Shelton, J. Y. Chan and S. M. Kauzlarich, *J. Appl. Phys.*, 1998, **83**, 7192.
- 8 X. Ma, J. Lu, J. B. Whalen and S. E. Latturmer, *Inorg. Chem.*, 2013, **52**, 3342–3348.
- 9 J. R. Salvador, D. Bilec, S. D. Mahanti, T. Hogan, F. Guo and M. G. Kanatzidis, *J. Am. Chem. Soc.*, 2004, **126**, 4474–4475.
- 10 P. H. Tobash and S. Bobev, *J. Am. Chem. Soc.*, 2006, **128**, 3532–3533.
- 11 F. Gascoin, S. Ottensmann, D. Stark, S. M. Haile and G. J. Snyder, *Adv. Funct. Mater.*, 2005, **15**, 1860–1864.
- 12 X. J. Wang, M. B. Tang, H. H. Chen, X. X. Yang, J. T. Zhao, U. Burkhardt and Y. Grin, *Appl. Phys. Lett.*, 2009, **94**, 092106.
- 13 A. Zevalkink, W. G. Zeier, G. Pomrehn, E. Schechtel, W. Tremel and G. J. Snyder, *Energy Environ. Sci.*, 2012, **5**, 9121–9128.
- 14 E. S. Toberer, A. F. May and G. J. Snyder, *Chem. Mater.*, 2010, **22**, 624–634.
- 15 B. Saparov, S.-Q. Xia and S. Bobev, *Inorg. Chem.*, 2008, **47**, 11237–11244.

- 16 J. Jiang, M. M. Olmstead, S. M. Kauzlarich, H.-O. Lee, P. Klavins and Z. Fisk, *Inorg. Chem.*, 2005, **44**, 5322–5327.
- 17 B. Eisenmann and Ute Rößler, *Z. Anorg. Allg. Chem.*, 1998, **624**, 406–410.
- 18 B. Eisenmann and H. Schäfer, *Angew. Chem.*, 1980, **19**, 480–481.
- 19 B. Eisenmann and H. Schäfer, *Z. Anorg. Allg. Chem.*, 1982, **484**, 142–152.
- 20 M. Khatun, S. S. Stoyko and A. Mar, *Inorg. Chem.* 2014, **53**, 7756–7762.
- 21 J. Wang, S.-Q. Xia and X.-T. Tao, *Inorg. Chem.*, 2012, **51**, 5771–5778.
- 22 B. Eisenmann, H. Jordan, H. Schäfer and Z. Naturforsch., *Teil B: Anorg. Chem.*, 1984, **39**, 1151–1153.
- 23 R. Lam and A. Mar, *Solid State Sci.*, 2001, **3**, 503–512.
- 24 G. Haegg and A. G. Hybinette, *Philos. Mag.*, 1935, **20**, 913–929.
- 25 W. Willott, E. Evans, *Philos. Mag.*, 1934, **18**, 114–128.
- 26 X. Liu, S. Xia, X. Lei, M. Pan, X. Tao, *Eur. J. Inorg. Chem.* 2014, **13**, 2248–2253.
- 27 S. Xia and S. Bobev, *J. Am. Chem. Soc.*, 2007, **129**, 4049–4057.
- 28 S.-J. Kim, S. Ponou and T. F. Fässler, *Inorg. Chem.*, 2008, **47**, 3594–3602.
- 29 P. Alemany, M. Llunell and E. Canadell, *Inorg. Chem.*, 2006, **45**, 7235–7241.
- 30 X. Liu, N. Lin, J. Wang, M. Pan, X. Zhao, X. Tao and S. Xia, *Inorg. Chem.*, 2013, **52**, 11836–11842.
- 31 S. S. Stoyko and A. Mar, *Inorg. Chem.*, 2011, **50**, 11152–11161.
- 32 Bruker APEX2; Bruker AXS Inc.: Madison, WI, 2005.
- 33 G. M. Sheldrick, SHELXTL; University of Göttingen: Göttingen, Germany, 2001.
- 34 E. Parthé and L. M. Gelato, *Acta Crystallogr.*, 1984, **A40**, 169.
- 35 L. M. Gelato, E. Parthé, *J. Appl. Crystallogr.*, 1987, **20**, 139.
- 36 G. K. H. Madsen, P. Blaha, K. Schwarz, E. Sjöstedt and L. Nordstrom, *Phys. Rev. B*, 2001, **64**, 195134.
- 37 K. Schwarz, P. Blaha and G. K. H. Madsen, *Comput. Phys. Commun.*, 2002, **147**, 71–76.
- 38 P. Blaha, K. Schwarz, G. K. H. Madsen, D. Kvasnicka and J. Luitz, *WIEN2k, An Augmented Plane Wave + Local Orbitals Program for Calculating Crystal Properties*, Technische Universität Vienna, Austria, 2001.
- 39 J. P. Perdew, S. Burke and M. Ernzerhof, *Phys. Rev. Lett.*, 1996, **77**, 3865–3868.